ACADEMIC PRESS

Available online at www.sciencedirect.com

SCIENCE DIRECT®

Journal of Sound and Vibration 260 (2003) 477–498

JOURNAL OF SOUND AND VIBRATION

www.elsevier.com/locate/jsvi

Reflection of sound at area expansions in a flow duct

S. Boij[a,*], B. Nilsson[b]

[a] *MWL, Department of Vehicle Engineering, Kungl Tekniska Högskolan, SE-100 44 Stockholm, Sweden*
[b] *School of Mathematics and Systems Engineering, Växjö University, SE-351 95 Växjö, Sweden*

Received 22 October 2001; accepted 4 April 2002

Abstract

An analytical model for scattering at area discontinuities and sharp edges in flow ducts and pipes is presented. The application we have in mind is large industrial duct systems, where sound attenuation by reactive and absorptive baffle silencers is of great importance. Such devices commonly have a rectangular cross-section, so the model is chosen as two-dimensional. Earlier solutions to this problem are reviewed in the paper. The modelling of the flow conditions downstream of the area expansion, with and without extended edges, and its implications for the resulting acoustic modes are discussed. Here, the scattering problem is solved with the Wiener–Hopf technique, and a Kutta condition is applied at the edge. The solution of the wave equation downstream of the expansion includes hydrodynamic waves, of which one is a growing wave. Theoretical results are compared with experimental data for the reflection coefficient for the plane wave, at frequencies below the cut-on for higher order modes. Influence of the interaction between the sound field and the flow field is discussed. A region where the reflection coefficient is strongly Strouhal number dependent is found.

1. Introduction

Sound propagation and scattering in ducts and pipes have gained increasing interest as the noise from duct systems, such as ventilation ducts, has become an increasing problem. Because of the super-imposed mean flow, the acoustics of such a duct system is more complex than for the non-flow case. For industrial applications, ducts with rectangular cross-section are commonly used, and reactive and absorptive baffle silencers are important devices to attenuate noise propagating in the system.

*Corresponding author. Tel.: +45-8-790-89-27; fax: +45-8-790-61-22.
E-mail address: susann@fkt.kth.se (S. Boij).

0022-460X/03/$ - see front matter
PII: S0022-460X(02)00950-1

In this paper, we present a method to determine scattering of sound at a flow duct area expansion with a possible extended edge. In particular, we are interested in the influence of the interaction between the sound field and the flow field at sharp edges in the duct. The model starts out from the one derived by Nilsson [1], where the scattering properties at the edge of a semi-infinite plate in a flow duct are studied. The model is based on the linear acoustic equations, including higher order acoustic modes. It is assumed that the flow conditions in the region close to the edge govern the flow—sound interaction [2–6]. Thus, for our purpose it is appropriate to model the velocity profile as a jet, i.e., the flow is not expanded in the region where the scattering is analysed. The modelling can be divided into three different parts: (a) mean velocity profiles and the introduction of a vortex sheet, (b) sound propagation in the straight duct parts and (c) the scattering at a sudden area change. The dissipation through interaction between the sound field and the flow field is of special interest, and can be studied with the models presented in this paper.

From the scattering properties of the splitter plate problem, it is possible to determine the scattering at an area expansion in a flow duct. In fact, it is possible to use the results for the splitter plate to construct the scattering properties of other geometrical changes as well. The synthesis is based on a building block technique [7]. The theoretical results are also compared with experimental data [2,8].

2. Background

Among the first attempts to describe the scattering properties of a flow duct area expansion is the work of Ronneberger [2]. The method is to apply linearized versions of the one-dimensional mass, energy and momentum conservation equations to a control volume. A similar model was presented by Alfredson and Davies [9]. Both these early models assumed an immediate expansion of the mean flow field after the area expansion. The justification for this assumption was that in the plane wave region, the wavelength is much longer than the length of the mixing region. Thus, the mixing region would be too small to influence the acoustic wave propagation. The dissipation due to the flow expansion is modelled as a change in the entropy. Based on the same fundamental acoustic equations is the model presented by Cummings [3]. The approach is to assume that the scattering occurs in a region where the flow has not yet expanded, and to assume entropy waves that allow for dissipation. However, it is concluded [10] that the presence of entropy waves can be neglected in this model, without major changes of the result. In these first low-frequency models all effects of higher order modes or near field effects are omitted by the way the low-frequency assumptions are applied.

The first attempt at a two-dimensional formulation for the acoustic field, including higher order modes, was the model presented by Nilsson and Brander [4,7,11,12]. This model is essentially the same as the one that forms the basis of the present article. The scattering properties of a bifurcated cylindrical duct, with a plug flow in the inner region, are studied. An exact model is formulated, including higher order acoustic modes, and hydrodynamic modes. The latter arise as a consequence of the sheared flow, modelled as an infinitely thin shear layer separating the core flow and the surrounding, quiescent medium. The scattering problem is formulated as Wiener–Hopf equations, which are solved to obtain the scattering properties. The solution satisfies the Kutta condition and causality requirements. The model also allows for an absorber in the outer region.

Finally, a building block method is presented, that indicates how the scattering properties of a number of discontinuities in series or in a more complicated arrangement can be deduced. Thus, area expansions, contractions and extended edges could be simulated.

A quantity of interest when describing the acoustic properties of the expansion is the impedance. The impedance is related to the phase of the reflection coefficient, so it is of interest to include any possible phase shift in the model. It has been argued that the flow field has no effect on the phase, but that it is mainly frequency dependent. This was put forward by Lambert and Steinbrueck [13] who presented a low-frequency – low Mach number model, including phase calculations. Peat [14] compared the impedance modelled by an analytical method and by FEM. In both models, the mean flow field is expanded immediately downstream of the expansion. Only convective effects on the acoustic field are included. The statement was that the magnitude of the reflection coefficient is Mach number dependent, whereas the phase shift is frequency dependent.

This is the basis for the plane wave model suggested by Davies [15]. The magnitude of the reflection coefficient should be derived including convective effects, and the phase would be derived from mode matching or as an end correction for a non-flow case. A model for this is presented by, e.g., Kergomard and Garcia [16], who formulate the end correction as a function of the area expansion ratio. In this paper, we will show that the phase is indeed dependent on both Mach number and frequency.

An extensive experimental work is that of Ronneberger [2,17], presenting results for the entire scattering matrix for an area expansion, including both magnitude and phase measurements. These results are still the best available in the literature, and are utilized in this paper. A modified one-dimensional model with vortex waves is presented along with a suggestion for a model including entropy waves. He also gives further arguments for the assumption that the interaction between sound field and flow field occurs before the jet has expanded. Aurégan [18] presented a model which is similar to that of Ronneberger [2] but includes a low-frequency approximation of the effects of the higher order modes through the achieved dispersion equation. The results for the magnitude of the reflection coefficient agree well with experimental results.

The effects of the vortex – sound interaction may also be described through an acoustic analogy where the vortex sheet is introduced as a source/sink term in the wave equation for the downstream duct. This approach was adopted by Dupère and Dowling [19], who investigated the sound absorbed by the vorticity field downstream of the area expansion. As the focus is on very low Mach number flow, it is argued that the Green function in the downstream duct can be determined for a fully expanded mean flow. Furthermore, a solution is constructed with the vortex sheet represented as a source term. It is also assumed that the shear layer is thick, so that the instability of the shear layer is avoided.

3. Scattering at the sharp trailing edge

In this section, reflection and transmission properties for a duct with a semi-infinite splitter plate will be presented. The aim is to apply the results to an area expansion in a two-dimensional (rectangular) flow duct, which is done in the next section. The area expansion can be a sudden step or include an extended edge, as depicted in Fig. 1. The flow field is such that the fluid in the lower part of the duct has a mean velocity $U_0 = Mc_0$, independent of y, while the flow in the upper part

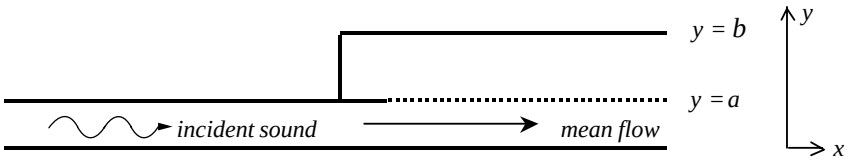

Fig. 1. A sound wave incident on an area expansion. A mean flow is present in the lower part of the duct, the dotted line indicating an infinitely thin shear layer.

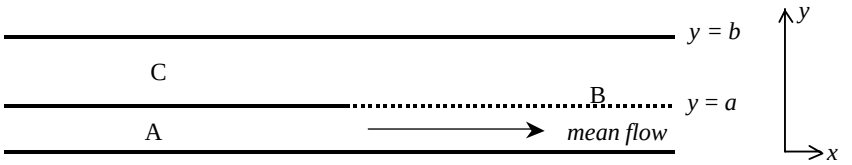

Fig. 2. Duct geometry for a trailing edge, where the dotted line represents the vortex sheet.

downstream of the expansion is quiescent. Then M, $0<M<1$, is the Mach number and c_0 is the speed of sound. The two regions are assumed to be separated by an infinitely thin shear layer, that is a vortex sheet. The problem is treated as linear, and viscous as well as thermal effects are neglected. As the scattering model that will be derived in the next section allows for an extended edge, there are three different regions involved, denoted A, B and C in Fig. 2. The solution to the problem in [1] is, for the readers convenience, presented in a self-contained form to allow for numerical computations.

An infinitely thin shear layer like the one in this model is unstable for all frequencies. This so-called Helmholtz instability is reflected in the solution of the wave equation through an unstable mode. Define the shear layer Strouhal number as

$$St = \frac{k\theta}{M}, \tag{1}$$

where θ is the thickness of the wall boundary layer close to the edge. The shear layer at the edge of the splitter plate is unstable when this Strouhal number is smaller than a critical value of about $\frac{1}{2}$ [20], and becomes stable for higher Strouhal numbers. Physically, the assumption of an infinitely thin shear layer is valid as long as the shear layer Strouhal number is well below this critical value.

3.1. Analytical model

The pressure solves the convective wave equation for the three regions. The walls are assumed rigid, and the displacement normal to the vortex sheet is assumed continuous. In ducts A and C, the wave numbers and mode shapes are, upon assuming a harmonic time dependence $\exp(-i\omega t)$,

$$\alpha_{An}^{\pm} = -\frac{kM}{(1-M^2)} \pm \frac{\sqrt{k^2-(1-M^2)(n\pi/a)^2}}{(1-M^2)}, \quad n = 0, 1, 2, \ldots, \tag{2}$$

$$\varphi_{An}(y) = \cos(n\pi y/a), \tag{3}$$

$$\pm\alpha_{Cn} \equiv \alpha_{Cn}^{\pm} = \pm\sqrt{k^2 - (n\pi/c)^2}, \quad n = 0, 1, 2, \ldots \tag{4}$$

$$\varphi_{Cn}(y) = \cos(n\pi(b - y)/c), \tag{5}$$

where $k = \omega/c_0$ is the wave number and a, b and c are the widths of ducts A, B and C. The square root is defined so that it has a positive imaginary part. In duct B, no explicit expression is found for the wave numbers $\alpha_{Bn}^{\pm}$, but they are solutions to the dispersion relation

$$G(\alpha) \equiv \frac{\cot hc}{h} + (1 - M\alpha/k)^2\frac{\cot Ha}{H} = 0, \tag{6}$$

where $H = \sqrt{(k - M\alpha)^2 - \alpha^2}$, $h = \sqrt{k^2 - \alpha^2}$. Let $H_{Bn}^{\pm}$ and $h_{Bn}^{\pm}$ denote H and h when $\alpha = \alpha_{Bn}^{\pm}$. The mode shape in duct B is

$$\varphi_{Bn}^{\pm}(\alpha_{Bn}^{\pm}, y) = \frac{1}{N(\alpha_{Bn}^{\pm})}\begin{cases} -\dfrac{(1 - M\alpha_{Bn}^{\pm}/k)^2}{H_{Bn}^{\pm}a \sin H_{Bn}^{\pm}a}\cos H_{Bn}^{\pm}y, & 0 < y < a, \\ \dfrac{1}{h_{Bn}^{\pm}a \sin h_{Bn}^{\pm}c}\cos h_{Bn}^{\pm}(b - y), & a < y < b, \end{cases} \tag{7}$$

where the mode shape is normalised so that the mean value of φ across the duct is one, thus

$$N(\alpha) = \frac{a}{b}\frac{M\alpha^3(M\alpha - 2k)}{(ka)^2(k^2 - \alpha^2)((k - M\alpha)^2 - \alpha^2)}. \tag{8}$$

It is worth commenting on the different wave types that appear in the solution. Besides the plane waves and the higher order acoustic modes, two other waves are also solutions of the equation. They are denoted hydrodynamic waves, as they propagate with a speed proportional to the mean flow rather than the speed of sound. Another feature is that the maximum of the amplitude at the vortex sheet gets sharper for increasing Strouhal number. Causality requirements yield that both waves propagate in the direction of the mean flow, and that one hydrodynamic wave is growing while the other one is a decaying wave. The exponential growth corresponds to the instability of the vortex sheet discussed above. After a certain distance, the amplitude of the growing wave becomes so large that the assumption of linearity is not valid. Physically, the instability wave breaks into turbulence. It is reasonable to neglect any interaction with the acoustic field in this region. Thus, our linear model includes the interaction at the edge, while any sound radiated from the breakdown into turbulence of the unstable shear layer is neglected.

A thorough analysis of the properties of the wave numbers is given in Ref. [21] and reviewed in Ref. [1]. A great advantage of the model is that there is a clear distinction between the three wave types; plane and higher order acoustic waves and hydrodynamic waves. For more involved models, for example with a continuously varying mean velocity profile, such a clear distinction would not be possible but the different modes would be of both acoustic and hydrodynamic nature. The only case when the current model could cause problems regarding the different wave types is if two wave numbers would merge for some special set of parameters. Then it would not be possible to track the wave type by continuation in some parameter. A case of special interest would be if the wave number of a leftward propagating higher order acoustic wave would merge

with the unstable hydrodynamic wave number. Then the convective instability would change into an absolute instability, and the model would break down as the stationary solution ceases to exist [1].

To derive the scattering coefficients, the Fourier transform is applied to the wave equations and the boundary conditions. Then Wiener–Hopf equations are formulated. To ensure uniqueness for the pressure, an edge condition is applied to the problem. For the trailing edge, as well as in the case of the area expansion, the flow forms a jet downstream of the area expansion. In both cases the Kutta edge condition, requiring [7]

$$\frac{\partial p}{\partial y}(x, a^+) = \mathrm{O}(x^{3/2}) \quad \text{when} \quad x \to 0^+, \tag{9}$$

is applicable. This is in contrast to the non-flow case, where the edge condition depends on the edge angle. The Kutta condition states that the velocity and the displacement are finite at the edge, and determines the strength of the scattered waves, in particular the amplitude of the hydrodynamic waves. This edge condition is physically relevant for small Strouhal number, St as defined in Eq. (1), for which the shear layer is unstable, as mentioned above.

The resulting scattering coefficients are organised in scattering matrices. Assume an incoming wave

$$P_A^{in} = \sum_n P_{A,n}^+ \varphi_{A,n}^+(y)\, \mathrm{e}^{\mathrm{i}\alpha_{A,n}^+ x} \tag{10}$$

from the left in duct part A, causing a transmitted wave

$$P_B^{tr} = \sum_n P_{B,n}^+ \varphi_{B,n}^+(y)\, \mathrm{e}^{\mathrm{i}\alpha_{B,n}^+ x}, \tag{11}$$

in duct B. The relation

$$P_{B,n}^+ = \sum T_{BAnm}^+ P_{A,m}^+ \tag{12}$$

defines the transfer matrix $\mathbf{T}_{BA}^+$. Upon introducing column vectors $\mathbf{P}_B^+$ and $\mathbf{P}_A^+$ with elements $P_{B,n}^+$ and $P_{A,n}^+$, relation (12) can be written $\mathbf{P}_B^+ = \mathbf{T}_{BA}^+ \mathbf{P}_A^+$. More generally, the transfer matrix $\mathbf{T}_{XY}^{\pm}$ describes the transmission from duct Y to duct X, while a reflection matrix $\mathbf{R}_X^{\pm}$ describes the reflection in duct X. The plus sign indicates that the scattered wave propagates to the right, while the minus sign indicates a leftward propagating scattered wave.

The trailing edge scattering coefficients required for the modelling of the area expansion in the next section are given below. For waves of mode order m originating in duct A, the scattering coefficients to waves of order n are

$$R_{Anm}^- = \frac{(-1)^m}{G_+(\alpha_{Am}^+) G_-(\alpha_{An}^-)} \frac{1}{(\alpha_{An}^- - \alpha_{Am}^+)} F_{An}^-, \tag{13}$$

$$T_{BAnm}^+ = \frac{a(-1)^m}{G_+(\alpha_{Am}^+)} \frac{1}{(\alpha_{Bn}^+ - \alpha_{Am}^+)} F_{Bn}^+, \tag{14}$$

$$T_{CAnm}^- = \frac{(-1)^m}{G_+(\alpha_{Am}^+) G_-(-\alpha_{Cn})} \frac{1}{(\alpha_{Cn} + \alpha_{Am}^+)} F_{Cn}^-, \tag{15}$$

and similarly for waves originating in duct C,

$$R^-_{Cnm} = -\frac{(-1)^m}{G_+(\alpha_{Cm})G_-(-\alpha_{Cn})}\frac{1}{(\alpha_{Cn}+\alpha_{Cm})}F^-_{Cn}, \tag{16}$$

$$T^+_{BCnm} = -\frac{a(-1)^m}{G_+(\alpha_{Cm})}\frac{1}{(\alpha^+_{Bn}-\alpha_{Cm})}F^+_{Bn}, \tag{17}$$

$$T^-_{ACnm} = -\frac{(-1)^m}{G_+(\alpha_{Cm})G_-(\alpha^-_{An})}\frac{1}{(\alpha^-_{An}-\alpha_{Cm})}F^-_{An}. \tag{18}$$

The functions $F^{\pm}_{Xn}$ are given by

$$F^-_{An} = \frac{(-1)^{n+1}(1-M\alpha^-_{An}/k)^2}{(1+\delta_{m0})a[(1-M^2)\alpha^-_{An}+Mk]},$$

$$F^+_{Bn} = N(\alpha^+_{Bn})\operatorname*{Res}_{\alpha=\alpha^+_{Bn}}\left[\frac{1}{G_-(\alpha)}\right],$$

$$F^-_{Cn} = \frac{(-1)^n}{(1+\delta_{n0})c\alpha_{Cn}},$$

where δ_{n0} is the Kronecker delta. The function $G(\alpha)$ can be written as a product,

$$G(\alpha) = G_+(\alpha)G_-(\alpha). \tag{19}$$

The plus factor is given by

$$G_+(\alpha) = \frac{(1-\alpha/\alpha^-_{B,pl})}{(1-\alpha/\alpha^-_{A,pl})(1-\alpha/\alpha^-_{C,pl})}M_+(\alpha)\sqrt{G(0)}, \tag{20}$$

and the minus factor is

$$G_-(\alpha) = \frac{(1-\alpha/\alpha^+_{B,gr})(1-\alpha/\alpha^+_{B,da})(1-\alpha/\alpha^+_{B,pl})}{(1-\alpha/\alpha^+_{A,pl})(1-\alpha/\alpha^+_{C,pl})}M_-(\alpha)\sqrt{G(0)}, \tag{21}$$

where the *pl* indicates the wave number of the plane wave, subscript *gr* indicates the growing hydrodynamic mode and subscript *da* the damped hydrodynamic mode. Finally, the factors M incorporate an infinite product

$$M_\pm(\alpha) = \prod_{n=1}^{\infty}\frac{(1-\alpha/\alpha^{\mp}_{Bn})}{(1-\alpha/\alpha^{\mp}_{An})(1-\alpha/\alpha^{\mp}_{Cn})}. \tag{22}$$

3.2. Numerical computations

Finally, in this section we describe how the transmission and reflection matrices (13)–(18) are computed. We take the reflection matrix R^-_{Anm} for duct A as an instructive example. The critical part is the computation of the infinite product (22) representing $G_+(\alpha^+_{Am})$ and $G_-(\alpha^-_{An})$. These infinite products are build from the wave numbers $\alpha^{\pm}_{An}$, $\alpha^{\pm}_{Cn}$ and$\alpha^{\pm}_{Bn}$. Only $\alpha^{\pm}_{Bn}$ require specific treatment in the form of a numerical solution of the zeros for $G(\alpha)$.

For very small ka, asymptotic expressions are available for all (infinitely many) zeros, and these are used as starting values. By increasing the frequency in small steps, the wave numbers for larger ka are found. The Newton–Raphson method is then used to determine the value of the wave numbers $\alpha_{Bn}^{\pm}$. Normally, the Newton–Raphson algorithm converges very quickly. For some parameter values there may be problems in that a zero jumps to another zero when ka is increased. Usually, this is resolved by choosing smaller steps in ka. If that remedy fails, the argument principle for analytic functions can be used to get information on the location of the zero. Still another method would be to use the method of steepest descent on $|G(\alpha)|$.

Having a method to compute the wave numbers $\alpha_{Bn}^{\pm}$, it remains to determine the infinite products $G_+(\alpha_{Am}^+)$ and $G_-(\alpha_{An}^-)$. Now, the accuracy of these infinite products can be checked in a very convenient way. From Eq. (19) it follows that $\varepsilon = |1 - G_-(\alpha)G_+(\alpha)/G(\alpha)|$ is a measure of the relative accuracy for $G_+(\alpha)$ and $G_-(\alpha)$. In actual fact ε is also a good measure on the relative accuracy on R_{Anm}^-. The relative error ε not being small is either an indication that a zero has jumped or that the number of factors in the truncated infinite product is too small. The convergence can be improved by estimating the part lost in truncation, using asymptotic methods [11]. However, this acceleration of convergence is not used in this report, since ordinary truncation is sufficiently fast. Our discussion was based on the matrix R_{Anm}^- (13). Obviously, all matrices can be analysed in a similar way.

4. Scattering at an area expansion with an extended edge

The results for the wave propagation and the results for the scattering at a sharp edge of a semi-infinite plate can now be used to find the acoustic properties of more complex geometries in a duct. To construct these, a building block method is used [7], and the basic idea is as follows. A duct part containing several discontinuities is first divided into basic elements, and the acoustic properties of each element are analysed. The properties of each part, or building block, are then combined so that the acoustic properties of the entire duct part can be described. The result is a transmission and a reflection matrix describing the duct part as one acoustic element.

We will now use the building block method to study the scattering from an area expansion with an extended edge. The geometry is achieved by closing of duct C by a vertical, acoustically rigid, wall a distance l from the edge of the splitter plate, as illustrated in Fig. 3. The geometry is denoted an area expansion with an extended trailing edge. Note that the model includes the special case when $l = 0$. There are two explanations for this. First, the Kutta edge condition is independent of the edge angle [7], as discussed above. Second, critical elements in the scattering matrices tend to zero in the low-frequency limit. This gives a good convergence of the model and

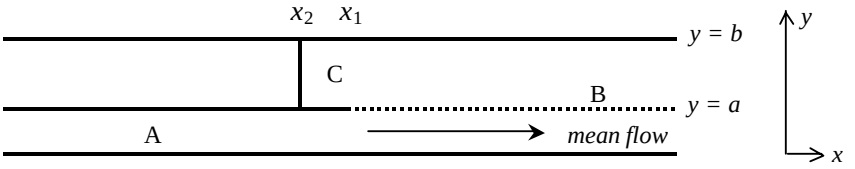

Fig. 3. A sudden area change with an extended edge of length $x_1 - x_2 = l$.

reduces the importance of the edge condition type. Consequently, the model converges when $l = 0$ even for the non-flow case, but the convergence is slower. Thus, the model can be used to compute the scattering properties of a sudden area expansion both with and without an extended inlet.

4.1. Scattering coefficients

We start by defining the scattering matrices. Let, as above, $\mathbf{P}^{\pm}$ be a column vector whose elements are the modal amplitudes P_n of a particular sound wave. A plus sign indicates propagation to the right and a minus sign propagation to the left. Thus $\mathbf{P}^{+}_{Ain}$ represents a wave in duct A propagating to the right impinging on the extended trailing edge, as shown in Fig. 3. Define the reflection matrix $\mathbf{R}^{-}$ and transmission matrix $\mathbf{T}^{+}$ by writing, for the resulting, unknown, pressure amplitudes $\mathbf{P}_A$ and $\mathbf{P}^{+}_B$ in ducts A and B, respectively,

$$\mathbf{P}_A = \mathbf{P}^{+}_{Ain} + \mathbf{R}^{-}\mathbf{P}^{+}_{Ain}, \tag{23}$$

and

$$\mathbf{P}^{+}_B = \mathbf{T}^{+}\mathbf{P}^{+}_{Ain}. \tag{24}$$

The matrices $\mathbf{R}^{-}$ and $\mathbf{T}^{+}$ can now [22] be expressed in terms of the scattering matrix elements in Section 3. The derivation yields

$$\begin{aligned}\mathbf{R}^{-} &= \mathbf{R}^{-}_A + \mathbf{T}^{-}_{AC}\mathbf{Q}^{-}_C(x_2, x_1)\mathbf{A}_C(x_1 - x_2)\mathbf{T}^{-}_{CA},,\\ \mathbf{T}^{+} &= \mathbf{T}^{+}_{BA} + \mathbf{T}^{+}_{BC}\mathbf{Q}^{-}_C(x_2, x_1)\mathbf{A}_C(x_1 - x_2)\mathbf{T}^{-}_{CA},\end{aligned} \tag{25}$$

where

$$\mathbf{Q}^{-}_C(x_2, x_1) = [1 - \mathbf{A}_C(x_1 - x_2)\mathbf{R}^{-}_C]^{-1}. \tag{26}$$

The reflection and transmission matrices on the right-hand of Eq. (25) are given in Eqs. (13)–(18). The factor $\mathbf{A}_C$ is a diagonal matrix representing the transmission path in duct C, whose diagonal elements are

$$\mathrm{e}^{-\mathrm{i}\alpha_{Cn}2(x_2 - x_1)}.$$

Under certain conditions, [7], it is possible to expand Eq. (26) as an infinite sum,

$$\mathbf{Q}^{-}_C(x_2, x_1) = [\mathbf{I} - \mathbf{A}_C(x_1 - x_2)\mathbf{R}_C]^{-1} = 1 + \mathbf{A}_C\mathbf{R}_C + (\mathbf{A}_C\mathbf{R}_C)^2 + \cdots. \tag{27}$$

Inserting expression (27) in, e.g., the expression for the transmission matrix $\mathbf{T}^{+}$, Eq. (25), yields

$$\mathbf{T}^{+} = \mathbf{T}^{+}_{BA} + \mathbf{T}^{+}_{BC}\mathbf{A}_C\mathbf{T}^{-}_{CA} + \mathbf{T}^{+}_{BC}\mathbf{A}_C\mathbf{R}_C\mathbf{A}_C\mathbf{T}^{-}_{CA} + \mathbf{T}^{+}_{BC}\mathbf{A}_C\mathbf{R}_C\mathbf{A}_C\mathbf{R}_C\mathbf{A}_C\mathbf{T}^{-}_{CA} + \cdots. \tag{28}$$

The factor $\mathbf{Q}^{-}_C\mathbf{A}_C$ can then be interpreted as representing the reflections between the plate edge and the end of the short duct part C. Eventually, these reflections will contribute to the scattered field in ducts A and B. In Fig. 4, the waves corresponding to the two first terms in (28) are shown, and it is indicated how the waves are partly transmitted to duct B and partly reflected into duct C. Apparently, the first term of the right-hand of Eq. (28) represents the portion of the wave that is directly reflected or transmitted at the point of scattering. Each following term can be interpreted as the part transmitted each time a wave has been reflected in duct part C. It is concluded that an infinite number of reflections at the wall in duct C are thus included in the analysis. Note that at each scattering event, an incident mode couples to all other modes.

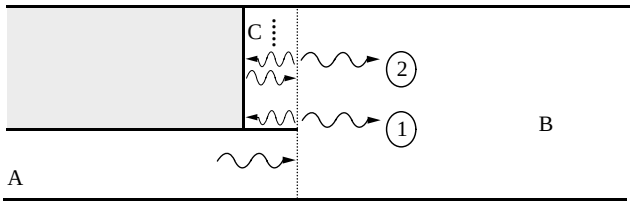

Fig. 4. The first two transmission paths for waves transmitted from duct A to duct B. The incident wave is scattered, step 1. The scattering give rise to one right going wave transmitted to duct B and one wave transmitted into the small closed duct part C. The latter is reflected at the wall and when it reaches the opening of the closed duct part, it is scattered, step 2; part of the wave is reflected and part is transmitted to duct B. The same process as in step 2 will now occur and will then repeat itself an infinite number of times.

The advantage of the original expression of $\mathbf{Q}_C^-$ is that the inverse matrix may very well exist and be finite even if the series in Eq. (27) does not converge. If that is the case, the interpretation of a sum of an infinite number of reflections is no longer valid.

The scattering of sound waves incident from duct A in the geometry depicted in Fig. 3 is then fully determined by the expressions in Eqs. (25). Together with the results for the wave propagation, these expressions give the acoustic properties of a flow duct with a sudden area expansion. Scattering coefficients for waves incident from downstream the area expansion can be derived in a similar way [22].

4.2. Numerical procedure

The computation of the scattering matrixes involves matrix multiplication, so it is important to include the appropriate number and choice of scattering coefficients to get the required accuracy, but also to keep the size of the matrices small. For the calculations in this paper the plane waves, the growing hydrodynamic wave in duct B and the least damped higher order waves have been chosen to build up 10×10 matrices. It may seem remarkable that very low order matrices can be used in the multiple scattering process. The reason is that critical scattering matrix elements tend to zero when kb tends to zero. This is the basis for a working quasi-stationary scattering theory as presented in Section 5. However, for increasing kb larger matrices are required. In addition, the computations of the matrices become much more time consuming for high frequencies.

5. Quasi-stationary model

A quasi-stationary version of the model has been derived [22]. In the quasi-stationary limit, it turns out that the scattering coefficients for the edge of the splitter plate depend only on the waves that propagate in this limit. In addition, it can be shown that critical scattering coefficients for all higher order modes tend to zero. Thus the only waves that have to be considered are the plane waves and the hydrodynamic waves, which propagate from zero frequency. For a trailing edge, five scattered waves are possible, as depicted in Fig. 5.

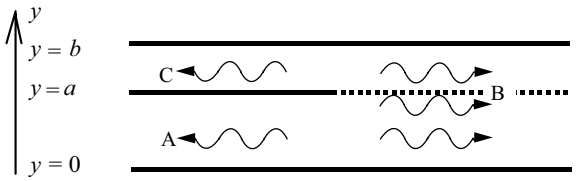

Fig. 5. Potential scattered waves at a trailing edge.

As an example, we give the resulting expression for the coefficient for plane wave reflection at a trailing edge back into duct A,

$$R_A^- = \frac{-\left(1-\frac{\alpha_{A,pl}^+}{\alpha_{C,pl}^-}\right)\left(1-\frac{\alpha_{A,pl}^-}{\alpha_{A,pl}^+}\right)\left(1-\frac{\alpha_{A,pl}^-}{\alpha_{C,pl}^+}\right)}{\left(1-\frac{\alpha_{A,pl}^+}{\alpha_{B,pl}^-}\right)\left(1-\frac{\alpha_{A,pl}^-}{\alpha_{B,gr}^+}\right)\left(1-\frac{\alpha_{A,pl}^-}{\alpha_{B,da}^+}\right)\left(1-\frac{\alpha_{A,pl}^-}{\alpha_{B,pl}^+}\right)} \frac{k^2 c\left(1-M\frac{\alpha_{A,pl}^-}{k}\right)^2}{2b[(1-M^2)\alpha_{A,pl}^- + Mk]\alpha_{A,pl}^-},$$

where the subscript *pl* indicates the wave number of the plane wave, the subscript *gr* indicates the growing hydrodynamic mode and subscript *da* the damped hydrodynamic mode. When the wave numbers are known, it is a straightforward procedure to calculate the reflection coefficient.

For ducts A and C we have the wave numbers

$$\begin{aligned}
\alpha_{A,pl}^+/k &= (1+M)^{-1},\\
\alpha_{A,pl}^-/k &= -(1-M)^{-1},\\
\alpha_{C,pl}^\pm/k &= \pm 1.
\end{aligned} \tag{29}$$

If only small Mach numbers are considered, the wave numbers in duct B can be expressed as a series for small M,

$$\begin{aligned}
\alpha_{B,pl}^+/k &= 1-\frac{a}{b}M+\left(a-\frac{3}{2}c\right)\frac{a}{b^2}M^2+\mathrm{O}(M^3) = (1+M\eta)^{-1}+\mathrm{O}(M^2),\\
\alpha_{B,pl}^-/k &= -1-\frac{a}{b}M-\left(a-\frac{3}{2}c\right)\frac{a}{b^2}M^2+\mathrm{O}(M^3) = -(1-M\eta)^{-1}+\mathrm{O}(M^2),,
\end{aligned} \tag{30}$$

where $\eta = a/b$ is the ratio between the cross-sections of the flow part and the wider part of the duct. Note here that the average mean flow over the cross-section of duct B is ηM. Although the velocity profile for the flow field in duct B is different from that of duct A, the correction of the wave numbers for the plane waves of duct B is of order M^2.

For the hydrodynamic waves in duct B we get

$$\begin{aligned}
\alpha_{B,gr}^+/k &= \left(1-\mathrm{i}\sqrt{\frac{a}{c}}\right)M^{-1}+\mathrm{O}(M),\\
\alpha_{B,da}^+/k &= \left(1+\mathrm{i}\sqrt{\frac{a}{c}}\right)M^{-1}+\mathrm{O}(M).
\end{aligned} \tag{31}$$

Scattering coefficients for the plane and hydrodynamic waves at an area expansion are derived following Section 4. The reflection coefficient for a wave incident downstream onto an area expansion with an extended edge is given by, upon assuming $kb \ll 1$,

$$r^- = -\frac{1-\eta}{\eta e^{ik2l}+1}\left[1+\frac{2\eta(1+e^{ik2l})}{\eta e^{ik2l}+1}M\right]+O(M^2). \tag{32}$$

The variable l is the length of the extended edge. If the length of the extended edge is set to zero, the reflection coefficient is

$$r^- = -\frac{1-\eta}{1+\eta}\left[1+\frac{4\eta}{1+\eta}M\right]+O(M^2), \quad \eta \leqslant 1. \tag{33}$$

This is the quasi-stationary limit for the plane wave reflection coefficient. Based on low-frequency theory for cylindrical ducts, Ronneberger [17] arrived at the same expression as Eq. (33), where η is the area ratio. In the current theory, the effect of higher order modes are included in the beginning, contrary to Ronneberger's model.

For small Mach numbers, the magnitude of reflection coefficient decreases with increasing η, corresponding to a decrease in area change. When η approaches one, i.e., no area change, the magnitude of reflection coefficient vanishes, as expected. Regarding an increase in the mean flow speed, the magnitude of the reflection coefficient increases with increasing Mach number. Note that the reflection coefficient is in agreement with the classical plane wave model when the Mach number is set to zero.

6. Results

6.1. Measurements and comparison method

To validate the model for scattering in a two-dimensional (rectangular) duct, we want to compare the theoretical results with experimental data. The measurements that we use are those performed by Ronneberger [8,2] on an area expansion in a cylindrical duct system with a non-reflecting termination. A mean flow field is built up along with the sound field. The sound pressure reflection and transmission properties of the area change are measured; Fig. 6. The three parameters that are varied are frequency, flow speed and the degree of area change. In this paper,

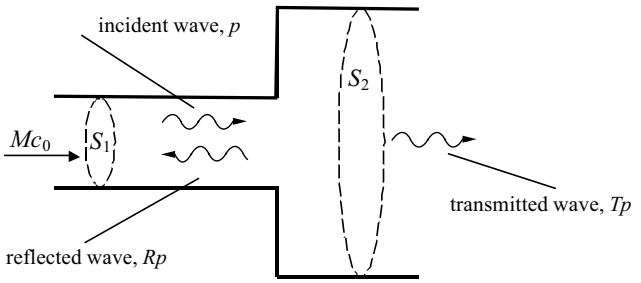

Fig. 6. Geometry of the measurement duct. Note that the downstream termination is non-reflecting. The amplitude of the reflected wave gives the value of the reflection coefficient.

we will focus on the reflection coefficients. Data for the transmission coefficient is also available, but the comparison will be left for a future publication.

The comparison of experimental results, for a cylindrical geometry, with theoretical results for a rectangular geometry, needs some further comments. The reason for the use of these experimental results is simply that they are the only experimental results available, where both magnitude and phase are measured. In addition, there are arguments for a correspondence between the cylindrical and the rectangular case. First, it should be noted that all measurements are performed in the plane wave region. When a plane wave is incident on an area expansion in a cylindrical duct, the pressure field at the entrance of the larger duct part is constant in the angular direction. Thus the only higher order modes that will be excited are the ones that are independent of the angular co-ordinate, but vary only as a function of the radius. These are commonly denoted radial modes. All this indicates that it is possible to consider the problem of wave propagation in cylindrical ducts, given the restrictions on parameters mentioned above, to be a two-dimensional problem. In that case, there is a correspondence to our theory for rectangular ducts, which has indeed a two-dimensional formulation as we ignore any influence of the depth of the duct.

One obvious problem in this context is the comparison of Helmholtz number, i.e., the dimensionless measure of the frequency. We argue that the predominant feature is the onset of higher order modes in the larger duct. For Helmholtz number far below the first cut-on of higher order modes, the wavelength is much larger than the transverse dimensions of the duct. Thus, the sound field will not resolve the geometrical details, and it can be assumed that the difference in geometry between a cylindrical duct and a rectangular duct will have a negligible influence on the scattering properties for plane waves. It could be expected that the plane wave reflection coefficient is reasonably similar for a cylindrical and a rectangular duct with the same area expansion ratio, if the frequency is normalised by the respective cut-on Helmholtz number.

The normalisation of the frequency is done as follows. The normalised Helmholtz number, here denoted He^*, is given by

$$He^* = \frac{kb}{(kb)_0} \tag{34}$$

where $(kb)_0$ is the cut-on Helmholtz number for the first higher order mode. It is given by $(kb)_{rec0} = \pi$ for the rectangular duct. For the cylindrical duct, $(kb)_0$ is given by the relation $J_0'(kb) = 0$ where J_0 is the zero order Bessel function, and the prime indicates the derivative of J_0 with respect to its argument. The solution is given numerically by $(kb)_{cyl0} = \kappa_0 \approx 3.832$.

It should also be noted that the geometrical parameter η, denoting the area expansion ratio, is different depending on the shape of the duct

$$\eta_{cyl} = \left.\frac{S_1}{S_2}\right|_{cyl} = \frac{r_a^2}{r_b^2}, \qquad \eta_{rec} = \left.\frac{S_1}{S_2}\right|_{rec} = \frac{a}{b}, \tag{35}$$

where r_a and r_b are the radii of the respective duct parts in the cylindrical duct, and a and b are the width of the respective duct parts in the rectangular duct. Now consider the case of a cylindrical and a rectangular duct with the same area expansion ratio η. Then we find the following relation

between ka for the rectangular and cylindrical duct:

$$He^* = \frac{1}{\eta}\frac{(ka)_{rec}}{\pi} = \frac{1}{\sqrt{\eta}}\frac{(ka)_{cyl}}{\kappa_0}. \tag{36}$$

6.2. Experimental and numerical results for the reflection coefficient

The presented theory is for scattering in rectangular ducts, and the available experimental data is, for reasons explained above, for cylindrical ducts. Thus, a comparison is to be regarded as qualitative in the first place. Nevertheless, as discussed in the previous section, the results can be expected to agree quantitatively as well, at least in the low-frequency region.

In this paper, we have chosen to concentrate on comparison with the reflection coefficient. First, low-frequency results for the reflection coefficient are presented. Dependence on area expansion ratio and on Mach number will be discussed. Next, results for frequencies up to 75% of the first cut-on frequency of higher order modes are presented. Frequency and Mach number dependence will be discussed, as well as a Strouhal number dependent phenomenon that is present in both experimental and theoretical data.

6.2.1. Low-frequency results for the magnitude of the reflection coefficient

We will first study the reflection coefficient at relatively low frequencies, well below the cut-on of any higher order modes. In this region, the magnitude of the reflection coefficient is almost independent of the frequency. We will refer to the quasi-stationary result for the reflection coefficient at low Mach number, expression (33). The frequency axis is normalised by the respective cut-on frequency for cylindrical and rectangular geometry. In Fig. 7, the magnitude of the reflection coefficient for two different area expansion ratios is shown. The predicted

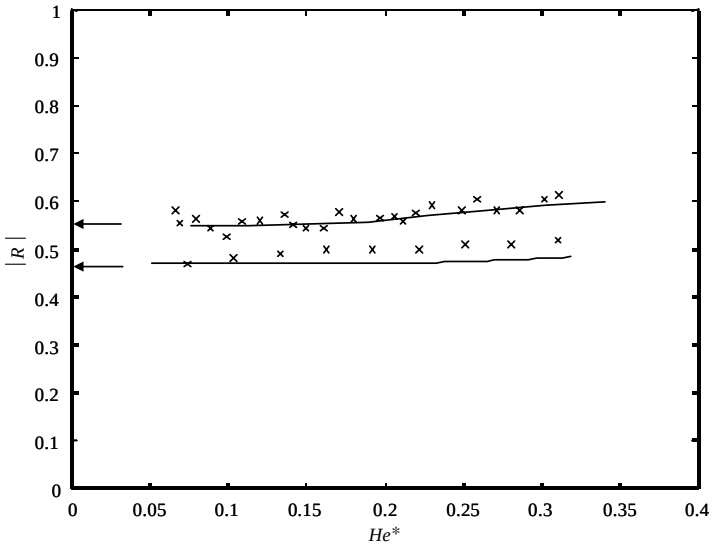

Fig. 7. Magnitude of the reflection coefficient R for the plane wave incident from duct A. $M = 0.3$, $\eta = 0.42$ (upper curve), $\times$, $\eta = 0.5$ (lower curve); $\times$, experiment [8]; —; full model result; ←: quasi-stationary result.

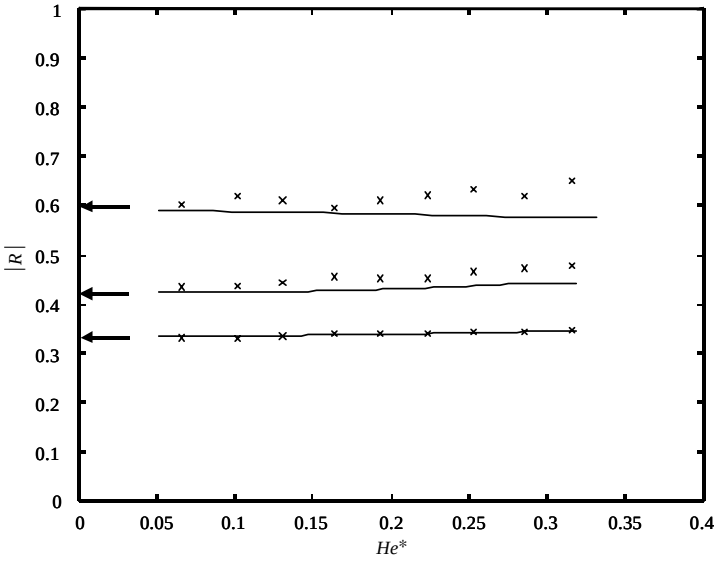

Fig. 8. Magnitude of the reflection coefficient R for the plane wave incident from duct A. $M = 0.001$ (lower), 0.2 (middle), 0.6 (upper) for theory and $M = 0, 0.2, 0.6$ for the experiment, $\eta = 0.5$; $\times$, experiment [8]; —, full model result; ←: quasi-stationary result.

dependence that the reflection decreases with increasing area expansion is verified by the experimental results. Furthermore, the calculated results, based on the general model, show very good agreement with the measured values. In Fig. 8, theoretical results are compared with experimental values of the magnitude of the reflection coefficient for three different Mach numbers for a fixed area expansion ratio. The results in Fig. 8 show that the model is continuous in the limit when M tends to zero. The magnitude of the reflection coefficient increases with increasing Mach number. The correspondence between computational and experimental results is good. As the Mach number increases, the calculated results seem to underestimate the reflection coefficient. It should also be noted that a higher flow speed would typically increase the measurement errors.

6.2.2. *The reflection coefficient as a function of the Mach number*

Here, theoretical values for the complex reflection coefficient are compared with experimental data [2], and the data is displayed as a function of the Mach number for some frequency values. The frequency ranges from 12.5% to 75% of the cut-on frequency of the first higher order mode, and the Mach number varies from 0 to 0.5. Data are given for the magnitude (Figs. 9–12), phase (Fig. 13), and as curves in the complex plane (Fig. 14).

From the magnitude and phase plots, we can see that the Mach number of the experiment seems to correspond to a slightly higher theoretical Mach number. This is also pointed out by the complex plot, where the theoretical and experimental curves coincide well, along the curves representing a fixed Helmholtz number. The discrepancy might be explained as follows. The velocity that determines the behaviour of the instability wave is the velocity outside of the wall boundary layers. In the case of the turbulent flow in the cylindrical pipe used in the experiment,

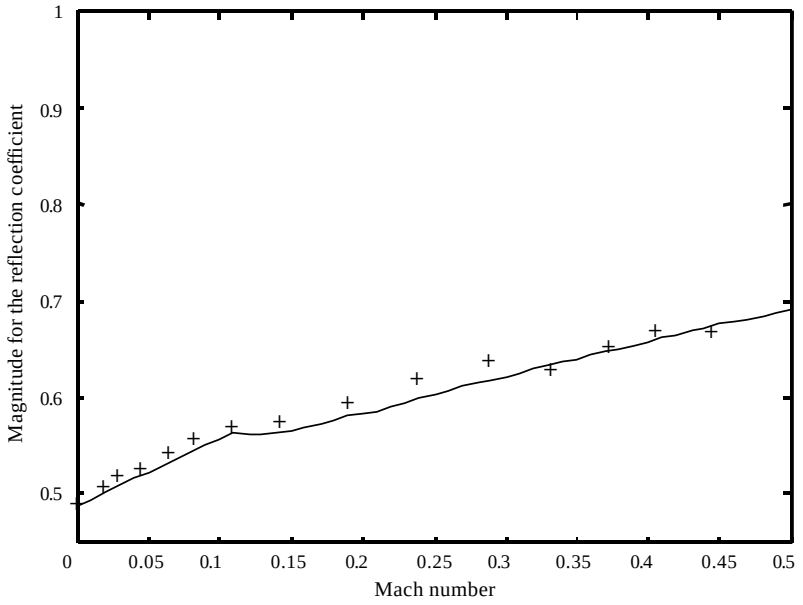

Fig. 9. The reflection coefficient of an area expansion, $\eta = 0.346$. The magnitude versus the Mach number M in the upstream part of the duct for $He^* = 0.125$. —, theory; +, experiment [2].

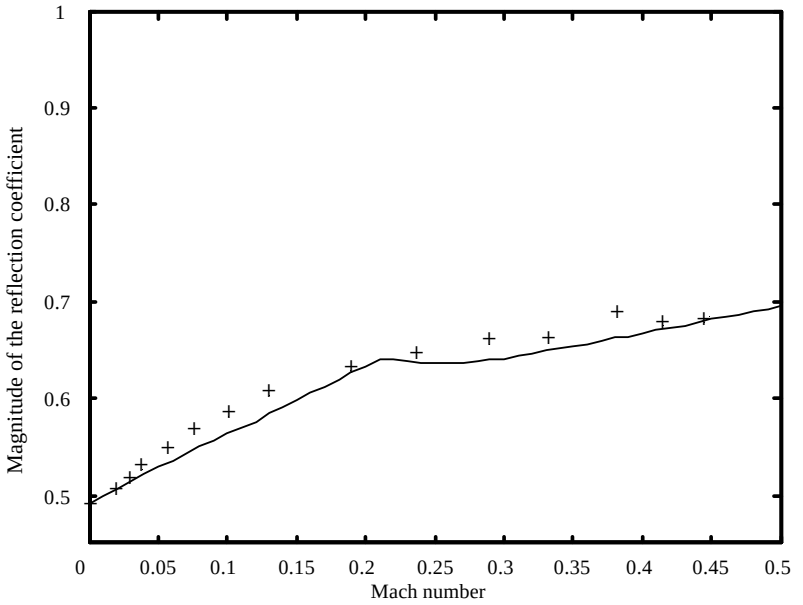

Fig. 10. The reflection coefficient of an area expansion, $\eta = 0.346$. The magnitude versus the Mach number M in the upstream part of the duct for $He^* = 0.25$. —, theory; +, experiment [2].

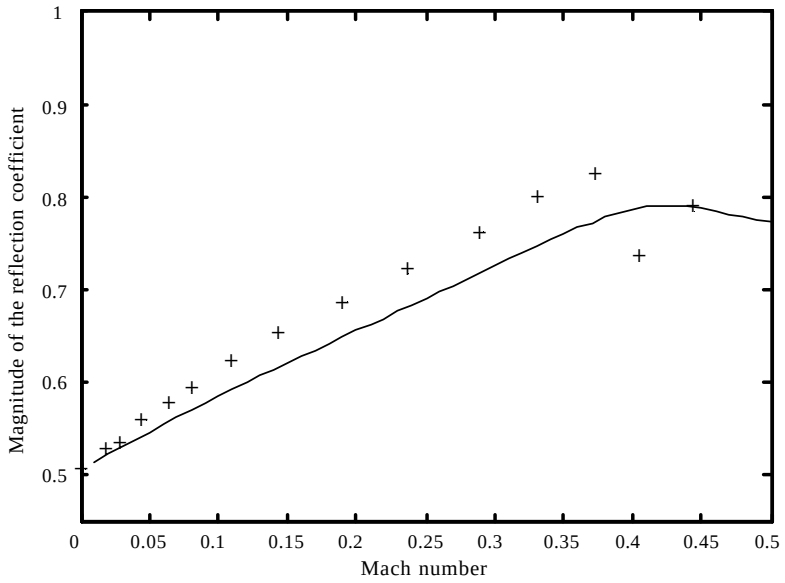

Fig. 11. The reflection coefficient of an area expansion, $\eta = 0.346$. The magnitude versus the Mach number M in the upstream part of the duct for $He^* = 0.50$. —, theory; +, experiment [2].

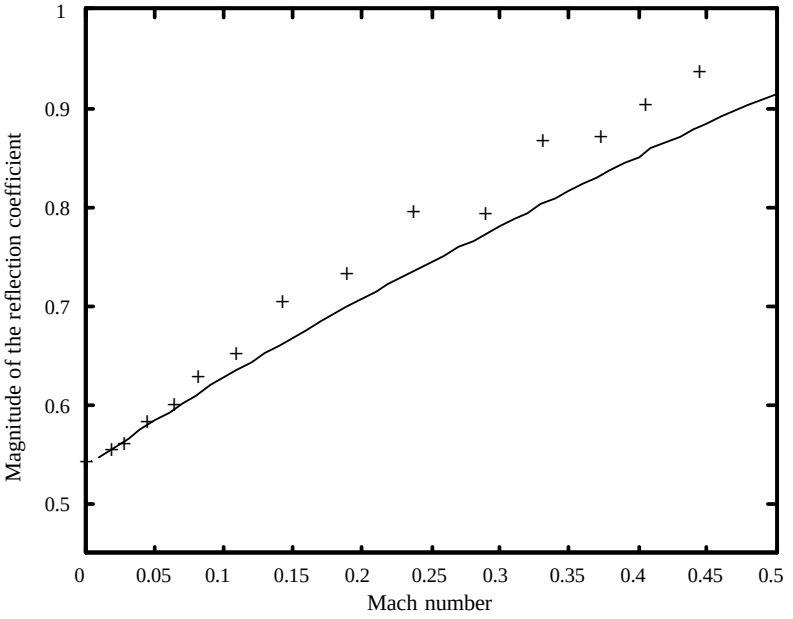

Fig. 12. The reflection coefficient of an area expansion, $\eta = 0.346$. The magnitude versus the Mach number M in the upstream part of the duct for $He^* = 0.75$. —; theory, +, experiment [2].

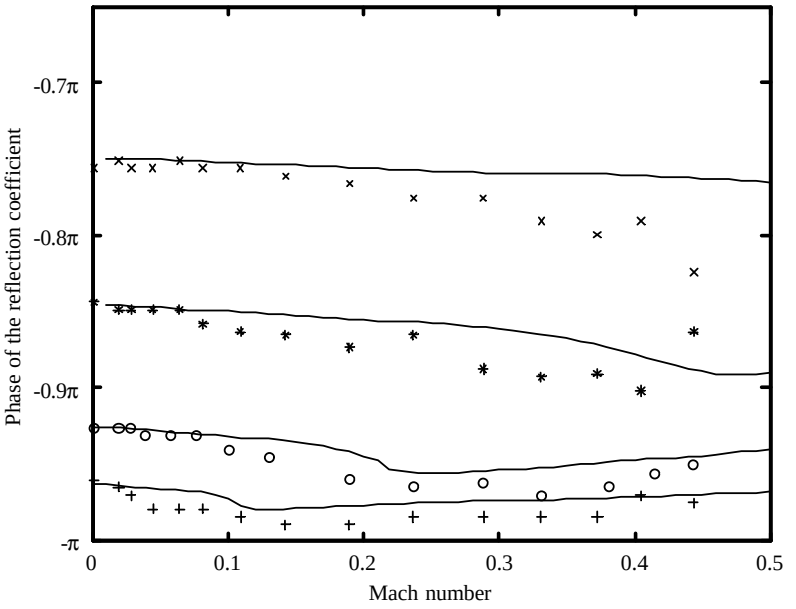

Fig. 13. The reflection coefficient of an area expansion, $\eta = 0.346$. The phase versus the Mach number M in the upstream part of the duct. —, theory, from the bottom $He^* = 0.125, 0.25, 0.5, 0.75$. Experiment [2]: +, He^*=0.125; o, He^*=0.25; *, He^*=0.5; ×, He^*=0.75.

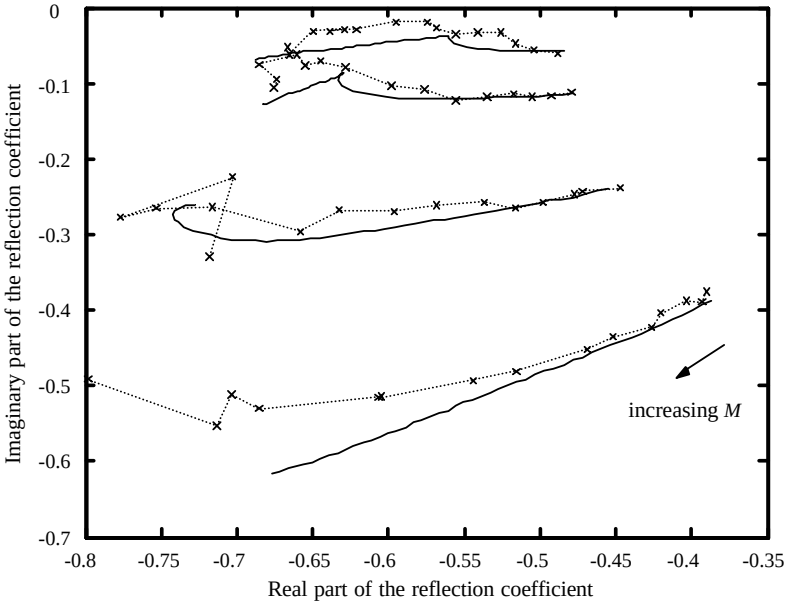

Fig. 14. The reflection coefficient as a function of Mach number in the complex plane. The Mach number range is 0.001–0.5. The curves are for, from above: $He^* = 0.125, 0.25, 0.5, 0.75$. —, theory; ×, Experiment [2] (The dotted line indicating the order of the data points.).

the Mach number is based on the mean value, rather than the value in the core. On the other hand, in the model, the boundary layers are neglected, so the theoretical Mach number corresponds to the velocity in the core. Thus, an experimental Mach number tends to correspond to a higher theoretical Mach number, as can be seen in the graphs. As an example for a turbulent flow in a circular duct, the difference between the maximum and the mean velocity is here around 20% [23].

The overall behaviour is that the magnitude is mainly dependent on Mach number whereas the phase is dependent on the frequency. Besides this main dependence, we can observe another phenomenon. For each frequency, the reflection coefficient shows a strong variation at a certain Mach number, and it turns out that this happens at a specific Strouhal number, ka/M. This is seen in the theoretical curves as well as in the experimental data. These results suggest that the interaction between sound field and flow field is particularly important when the Strouhal number is close to one. Apparently, our theory predicts this phenomenon.

6.2.3. *Frequency dependence in the reflection coefficient*

In this section, the reflection coefficient is studied as a function of the frequency, for some fixed Mach numbers. In Figs. 15 and 16, the magnitude and the phase of the reflection coefficient for a sudden area expansion are shown. The magnitude typically increases to reach a peak value close to the cut-on frequency, $He^* = 1$, for the first higher order mode in the downstream duct B. When this mode starts to propagate in duct B, the reflection coefficient for the plane wave mode drops quickly. As in the previous section, we can observe a strong Strouhal number dependence in a region around $St = ka/M = 1$. Thus, this phenomenon cannot be modelled by the quasi-stationary theory. There, ka is assumed to reach zero in a specific sense, implying that the Mach number must be larger than ka.

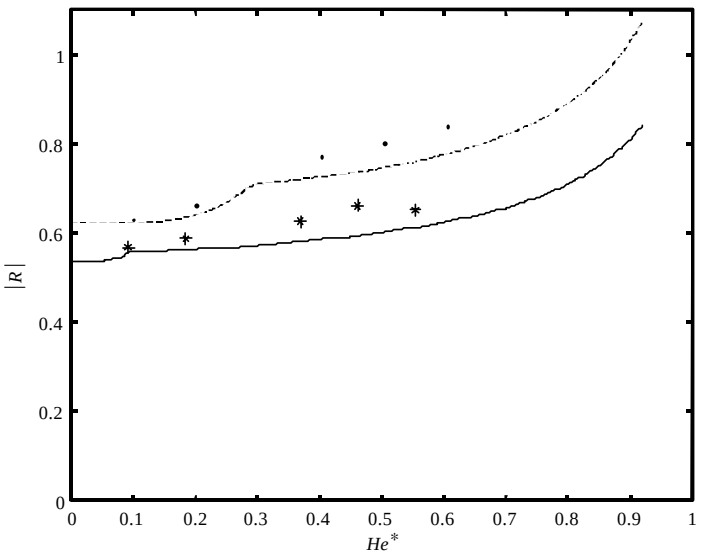

Fig. 15. Magnitude of the reflection coefficient for the plane wave incident from duct A for $\eta = 0.35$. Experiment [2]: $*$, $M = 0.1$; ●, $M = 0.3$; Theory: —, $M = 0.1$; - - -, $M = 0.3$.

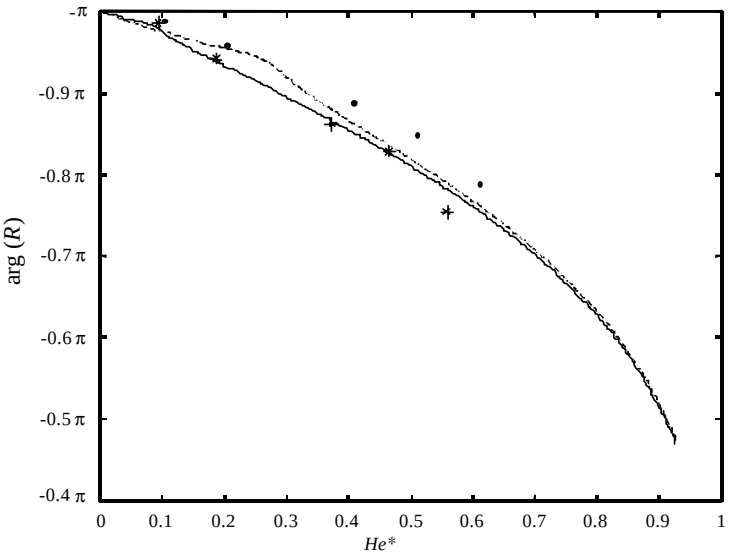

Fig. 16. Phase of reflection coefficient R for the plane wave incident from duct A for $\eta = 0.35$. Experiment [2]: $*$, $M = 0.1$; ●, $M = 0.3$; Theory: —; $M = 0.1$; - - -, M=0.3.

The Mach numbers of the theoretical and the experimental data seem to differ somewhat, as mentioned in the previous section where an explanation was suggested. Despite this, the graphs show that the frequency dependence of the magnitude of the reflection coefficient is important as we approach the first cut-on frequency. The good agreement between the calculated and measured phase justifies the frequency normalization scheme described in Section 6.1. It implies that our comparison of measurements on a cylindrical geometry with calculations on a rectangular geometry is acceptable. It also further supports the validity of the assumption that the shape of the cross-section has little influence on the scattering properties at low frequencies [2].

7. Summary and conclusions

The scattering properties of a flow duct area expansion have been studied, and earlier works have been reviewed. An analytical two-dimensional model [1], which treats general scattering properties of bifurcated ducts, with the focus on the sound field – flow field interaction, has been presented. The acoustic field is modelled with an infinite number of modes. In order to construct more complicated duct elements, a building block method [7] is applied to the result of this canonical problem. In this case, the model is applied to an area expansion. A quasi-stationary version of the model is also derived, and explicit formulas are given in the case of small Mach number. A comparison with experimental data [8,2], verifies the model, and results are especially good in the low-frequency region, even for Mach numbers as high as 0.6. It should be noted that the experimental results available are for a cylindrical geometry. To overcome this problem, a frequency normalization scheme (based on the first cut-on frequency in the larger duct) is

suggested. Two features of the reflection coefficient should be noted. For a fixed frequency, the Mach number of the experimental results corresponds to theoretical results of a slightly higher Mach number. An interesting interpretation is that it is the Mach number of the main core of the turbulent flow, rather than the Mach number based on the mean velocity that determines the behaviour of the instability wave. The second phenomenon is a strong variation in the reflection coefficient, apparent in both computed and experimental results. It appears at a Strouhal number (based on the duct width) of about one. It indicates that the interaction between the sound field and the sheared flow at the edge of the area expansion is particularly important in this Strouhal number region. Further implications of this phenomenon are well worth studying. It would also be of interest to study the influence of the Kutta condition on the results.

References

[1] B. Nilsson, Scattering of stable and unstable waves in a flow duct, Quarterly Journal of Mechanics and Applied Mathematics 51 (1998) 599–632.
[2] D. Ronneberger, Theoretische und experimentelle Untersuchung der Schallausbreitung durch Querschnittssprünge und Lochplatten in Strömungskanälen, DFG-Abschlussbericht, Drittes Physikalisches Institut der Universität Göttingen, Göttingen, 1987.
[3] A. Cummings, Sound transmission at sudden area expansions in circular ducts, with superimposed mean flow, Journal of Sound and Vibration 38 (1975) 149–155.
[4] B. Nilsson, O. Brander, The propagation of sound in cylindrical ducts with mean flow and bulk-reacting lining – I. Modes in an infinite duct, Journal of the Institute of Mathematics and its Applications 26 (1980) 269–298.
[5] R.M. Munt, Acoustic transmission properties of a jet pipe with subsonic jet flow: I. The cold jet reflection coefficient, Journal of Sound and Vibration 142 (1990) 413–436.
[6] M.S. Howe, Attenuation of sound in a low Mach number nozzle flow, Journal of Fluid Mechanics 91 (1979) 209–229.
[7] B. Nilsson, O. Brander, The propagation of sound in cylindrical ducts with mean flow and bulk-reacting lining — IV. Several interacting discontinuities, IMA Journal of Applied Mathematics 27 (1981) 263–289.
[8] D. Ronneberger, Experimentelle untersuchungen zum akustischen reflexionsfaktor von unstetigen querschnittsänderung in einem luftdurchströmten rohr, Acustica 19 (1967/68) 222–235.
[9] R.J. Alfredson, P.O.A.L. Davies, Performance of exhaust silencer components, Journal of Sound and Vibration 15 (1971) 175–196.
[10] A. Cummings, H. Haddad, Sudden area changes in flow ducts: further thoughts, Journal of Sound and Vibration 54 (1977) 611–612.
[11] B. Nilsson, O. Brander, The propagation of sound in cylindrical ducts with mean flow and bulk-reacting lining — II. Bifurcated ducts, Journal of the Institute of Mathematics and its Applications 26 (1980) 381–410.
[12] B. Nilsson, O. Brander, The propagation of sound in cylindrical ducts with mean flow and bulk-reacting lining — III. Step discontinuities, IMA Journal of Applied Mathematics 27 (1981) 105–131.
[13] R.F. Lambert, E.A. Steinbrueck, Acoustic synthesis of a flowduct area discontinuity, Journal of the Acoustical Society of America 67 (1980) 59–65.
[14] K.S. Peat, The acoustical impedance at discontinuities of ducts in the presence of a mean flow, Journal of Sound and Vibration 127 (1988) 123–132.
[15] P.O.A.L. Davies, Practical flow duct acoustics, Journal of Sound and Vibration 124 (1988) 91–115.
[16] J. Kergomard, A. Garcia, Simple discontinuities in acoustic waveguides at low frequencies: critical analysis and formulae, Journal of Sound and Vibration 114 (1987) 465–479.
[17] D. Ronneberger, Zur Kutta-bedingung bei der Schallausbreitung durch durchströmte Quersnittssprünge und Lochplatten, Proc. DAGA '89, 1989.

[18] Y. Aurégan, Comportement aéro-acoustique basse-fréquence d'une expansion, 14e Congrès Français de Mécanique, Toulouse, 1999.
[19] I.D.I. Dupère, A.P. Dowling, The absorption of sound near axisymmetric area expansions, Journal of Sound and Vibration 239 (2001) 709–730.
[20] A. Michalke, On spatially growing disturbances in an inviscid shear layer, Journal of Fluid Mechanics 23 (1965) 521–544.
[21] B. Nilsson, Stable and unstable waves in a flow duct. Part I: Green's function, Report 10, Växjö University-Mathematics, Natural Sciences and Technology, 1998.
[22] S. Boij, Mean Flow Effects on the Acoustics of Silencers, Licentiate Thesis, KTH, Stockholm, 1999.
[23] H. Schlichting, Boundary Layer Theory, McGraw-Hill, New York, 1968.